Supplemental Material: Resonant inelastic X-ray scattering investigation of Hund's and spin-orbit coupling in $5d^2$ double perovskites

Felix I. Frontini,[1,*] Christopher J. S. Heath,[1] Bo Yuan,[1,†] Corey M. Thompson,[2,‡] John Greedan,[2,3] Adam J. Hauser,[4] F. Y. Yang,[5] Mark P. M. Dean,[6] Mary H. Upton,[7] Diego M. Casa,[7] and Young-June Kim[1,§]

[1]*Physics Department, University of Toronto, 60 St. George Street, Toronto, ON, M5S 1A7*
[2]*Department of Chemistry and Chemical Biology, McMaster University, Hamilton, Ontario, Canada L8S 4L8*
[3]*Brockhouse Institute for Materials Research, McMaster University, Hamilton, Ontario, Canada L8S 4L8*
[4]*Department of Physics and Astronomy, The University of Alabama, Tuscaloosa, Alabama 35487, USA*
[5]*Department of Physics, The Ohio State University, Columbus, Ohio 43210, USA*
[6]*Department of Condensed Matter Physics and Materials Science, Brookhaven National Laboratory, Upton, New York 11973, USA*
[7]*Advanced Photon Source, Argonne National Laboratory, 9700 S. Cass Avenue, Lemont, IL 60439*

(Dated: September 11, 2025)

S-I. ADDITIONAL Ba_2YReO_6 RESULTS

A. Elastic normalized data

The Re L_2 and L_3 edge RIXS spectra of Ba_2YReO_6 obtained at resonance maximum are plotted in Fig. S1 using different normalization schemes. The left and right panel are normalized by the elastic line and 0.5 eV feature, respectively. The elastic line normalization clearly illustrates that the atomic features at $\sim$ 0.5 eV, 0.9 eV and 1.8 eV

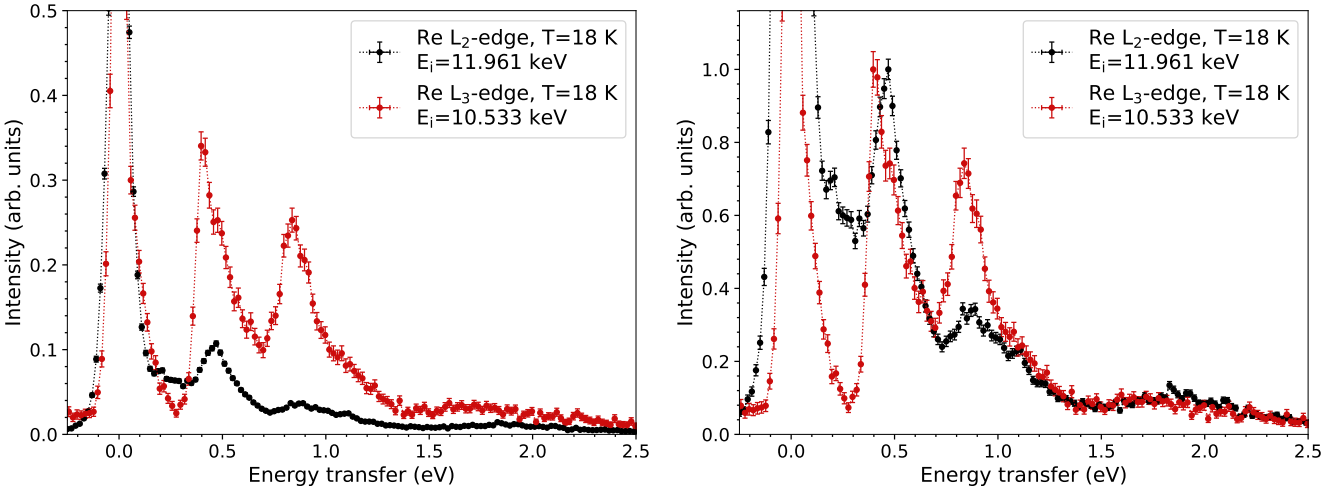

FIG. S1. Ba_2YReO_6 RIXS spectra at the Re L_2 and L_3 edge resonances up to 2.5 eV in E_t collected at T = 18 K. The RIXS spectra are normalized by the maximum intensity of the elastic line (left) and the 0.5 eV feature (right).

are significantly suppressed relative to the elastic line at the L_2 edge. On the other hand, the data also shows that the low energy region is enhanced at the L_2 edge even under the elastic line normalization scheme.

* ffrontini@anl.gov; Present address: Advanced Photon Source, Argonne National Laboratory, 9700 S. Cass Avenue, Lemont, IL 60439
† Present address: Department of Physics and Astronomy, McMaster University, Hamilton, Ontario L8S 4M1, Canada
‡ Present address: Department of Chemistry, Purdue University, 560 Oval Drive, West Lafayette, Indiana 47907-2084, USA
§ youngjune.kim@utoronto.ca

B. Resonance behavior

The low energy region was shown to be resonantly enhanced at the L_3 edge in the main document but this behavior is less clear at the L_2 edge in the RIXS map, hence we plot the E_i dependence of line cuts in Fig. S2. The Re L_2 and L_3 edge RIXS spectra of Ba_2YReO_6 are shown as a function of E_i in Fig. S2, normalized by the beam monitor, which shows that the low energy feature around 0.1-0.2 eV resonates at both edges.

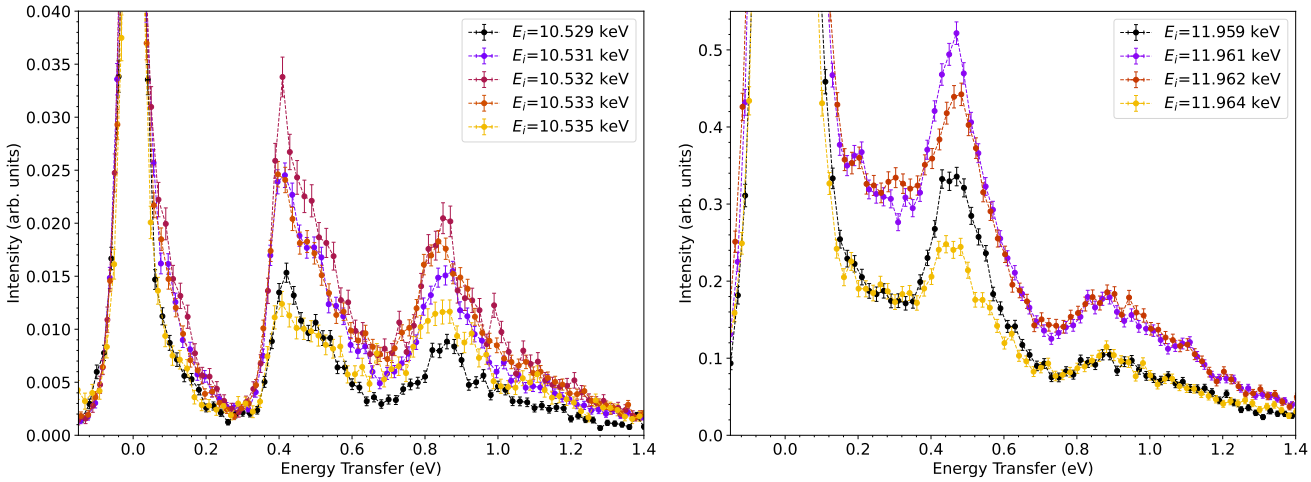

FIG. S2. E_i dependence of the Ba_2YReO_6 RIXS spectra up to 1.4 eV in E_t at (left) the Re L_3 edge and (right) the Re L_2 edge. Data were collected at T = 18 K.

Moreover, we also see that the intensity is slightly higher for E_i = 10.532 keV, while the high-statistics data shown in the main text was obtained 10.533 keV.

C. Temperature dependence

In addition to our edge-dependent measurements at low temperatures we collected limited temperature dependence measurements at the Re L_2 edge, shown in Fig. S2. Both subplots show that the 0.9 eV and 1.8 eV features appear to

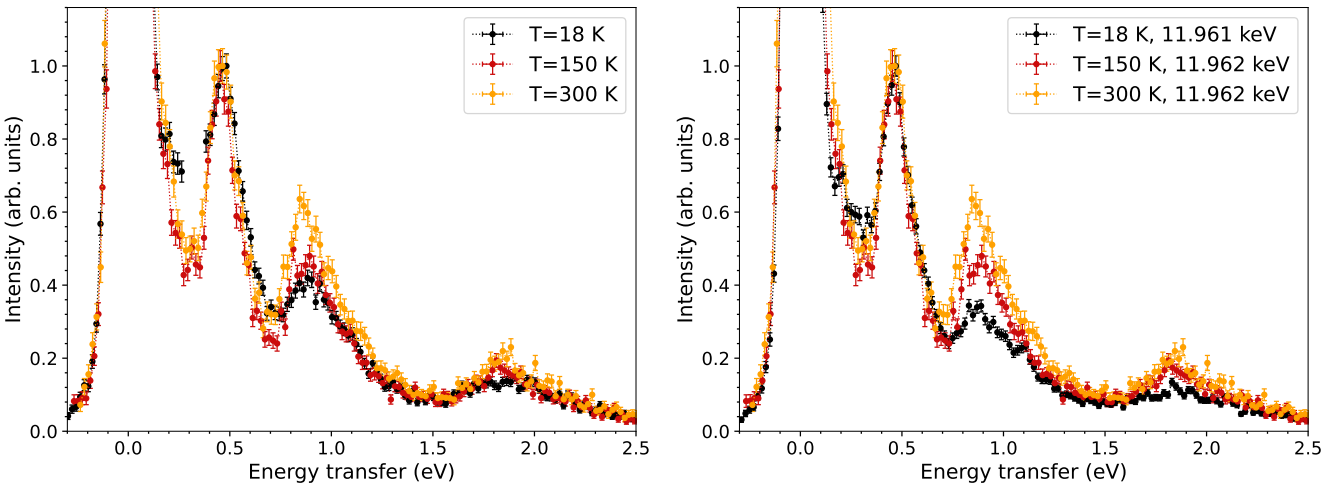

FIG. S3. Ba_2YReO_6 Re L_2 edge RIXS spectra up to 2.5 eV in E_t as a function of temperature. The spectra in the left subplot are all collected at E_i=11.962 keV and are normalized by the maximum intensity of the 0.5 eV feature. The region between 0.27 eV and 0.38 eV is removed from the T = 18 K dataset due to a non-physical artefact, likely due to a cosmic ray background. In the right subplot, we swap out the corrupted low-temperature scan with the scan at 11.961 keV.

display some slight temperature evolution relative to the 0.5 eV feature. The feature intensities appear to be slightly enhanced at high temperature but the features retain the same shape, such that this enhancement may be spurious. Additionally, the low statistics of the high temperature data make it difficult to comment confidently on whether the perceived differences are statistically significant. Of note, no large changes are observed across the phase transition temperatures at $T_l = 31$ K and $T_u = 37$ K.

S-II. ADDITIONAL Sr_2CrReO_6 RESULTS

A. Resonance behavior

E_i dependence of the low energy Re L_2 and L_3 edge RIXS spectra of Sr_2CrReO_6 is shown in Fig. S4, normalized by the beam monitor. Fig. S4 shows that both the continuum features and atomic-like *dd* excitations are resonantly

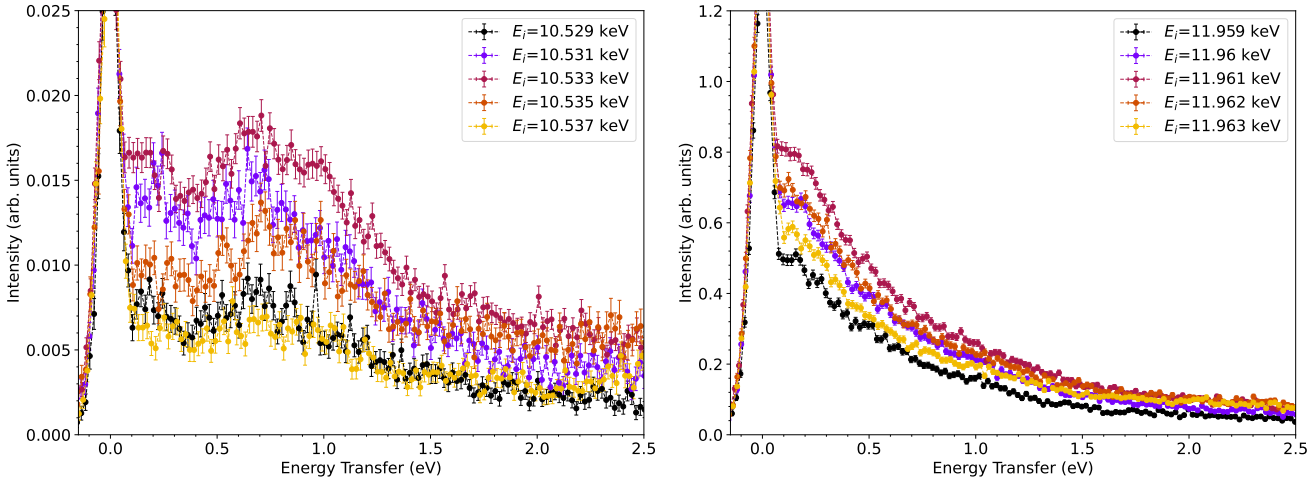

FIG. S4. E_i dependence of the Sr_2CrReO_6 RIXS spectra up to 2.5 eV in E_t at the Re L_3 edge (left) and the Re L_2 edge (right). Data were collected at T = 300 K.

enhanced. The resonance behavior of high-energy features at the L_2 edge is also shown as line scans in Fig. S5, normalized by the beam monitor. Fig. S5 shows, as discussed in the main text, that the e_g CEF transition around

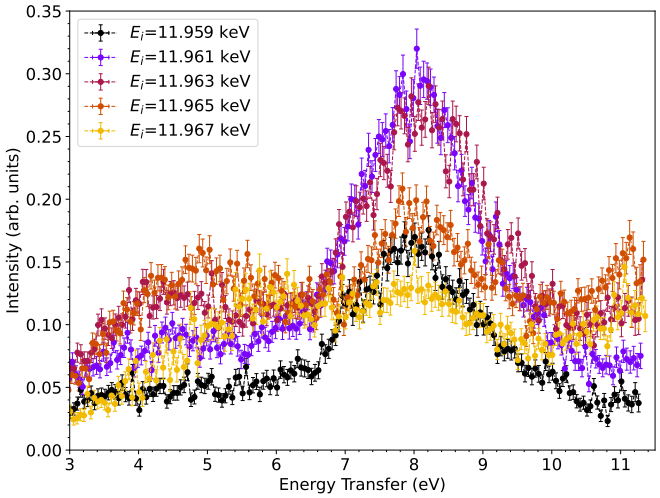

FIG. S5. E_i dependence of the Sr_2CrReO_6 RIXS spectra up to 11.5 eV in E_t at the Re L_2 edge. Data were collected at T = 300 K.

E_t =4.5 eV resonates at 11.965 keV, whereas the low energy features and charge-transfer feature around E_t =8 eV

resonate at 11.961 keV. Moreover, the linescans show more clearly that the high energy feature partially visible above 10 eV also resonate at 11.965 keV, marking them as CEF+charge-transfer excitations.

S-III. RIXS CALCULATIONS

Theoretical RIXS spectra of Ba_2YReO_6 were calculated using atomic multiplet theory of the $5d^2$ system implemented in the EDRIXS package (version 0.1.1) [S1]. The model Hamiltonian for this system is solved by exact diagonalization (ED) in the Fock basis. Within this basis the Coulomb interaction is parameterized by the Slater integrals for dd electron interactions (F^0_{dd}, F^2_{dd}, F^4_{dd}) and dp electron-hole interactions (F^2_{pd}, G^1_{pd}, G^3_{pd}). F^0_{dd}, F^2_{dd}, and F^4_{dd} are derived from onsite Coulomb interaction strength (U_d) and the Hund's coupling (J_H), where U_d is a free parameter as RIXS is a charge-neutral process and the absolute resonant incident energy is scaled to match experimental observations.

F^2_{pd}, G^1_{pd}, G^3_{pd} were taken from the Hartree-Fock atomic structure code originally developed by R. D. Cowan [S2] and rescaled to account for nephelauxetic reduction [S3]. The nephelauxetic reduction factor was investigated as a free parameter and was found to be optimal in the range of 0.85 - 1.00 with only small deviations within that regime. A value of 0.9 was used for subsequent calculations. SOC for the $2p$ core hole (1005.839 eV) was similarly taken from atomic calculations using the Cowan code [S2]. The SOC for the $5d$ valence electrons (ζ) and the Hund's coupling (J_H) were investigated as additional free parameters and a heatmap comparing the calculated spectra to the experimental data is shown in Fig. S7. The heatmaps show two different metrics, one for comparing how well the peak energies match (right) and one for comparing the spectral intensities (left). Of these two metrics, the peak energies metric optimizes values which better represent the experimental data. As discussed in the main text, the optimal values ($\zeta = 0.29$ eV, $J_H/\zeta = 1.30$) are selected to balance contributions from the L_2 and L_3 edges, as they are slightly misaligned relative to one another when compared with the calculated spectra. The optimal J_H represents a reduction factor of 0.37 compared to the atomic Hartree-Fock value given by the Cowan code.

A cubic crystal field term was included, with 10Dq set to 4.5 eV based on the observed splitting of the e_g and t_{2g} levels of Sr_2CrReO_6, matching previous experimental results [S4]. The finite crystal field results in a splitting of the $J_{eff} = 2$ quintet by ~ 15 meV, which can be seen in the calculated low energy RIXS spectra at the L_2 and L_3 edges shown in Fig. S6. Variations of 10Dq within the physical range of 4.5-5 eV did not meaningfully alter the peak positions in the spectra (maximum variation of ~ 8 meV and average variation of ~ 4 meV).

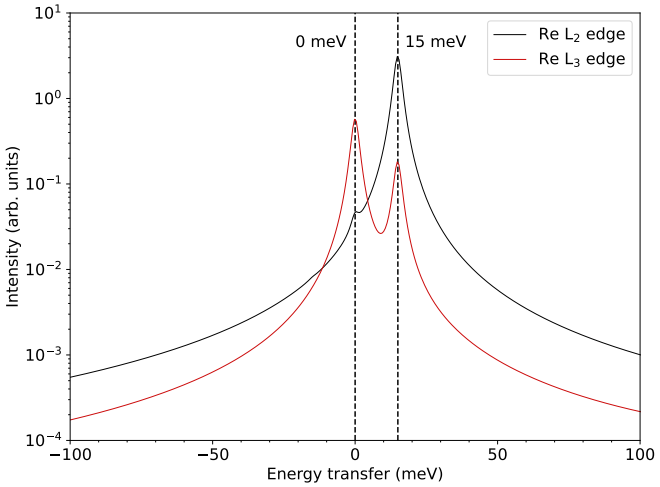

FIG. S6. EDRIXS calculated low energy RIXS spectra of Ba_2YReO_6 at the L_2 and L_3 edge. The spectra are minimally broadened to a FWHM of 3 meV and shown in log scale to showcase the ~ 15 meV splitting of the $J_{eff} = 2$ quintet.

The calculation of the RIXS cross section used a core-hole life-time broadening factor for the incident energy of 2.345 eV for the L_3 edge and 2.71 eV for the L_2 edge taken from the Cowan Hartree-Fock calculations. In the plots shown in Fig. 5 of the main text, a Lorentzian broadening of 15 meV was used for the energy transfer in order to clearly distinguish the excitations in the spectra. Additional Gaussian instrumental broadening of 95 meV FWHM for L_2 and 65 meV FWHM for L_3 was included when comparing calculated spectra to experimental data. An arbitrarily large Gaussian broadening of 350 meV FWHM was used to account for the short lived $^1S_0$ excitation near 2 eV. The temperature (18 K), polarization conditions, and scattering geometry were matched to the experimental setup.

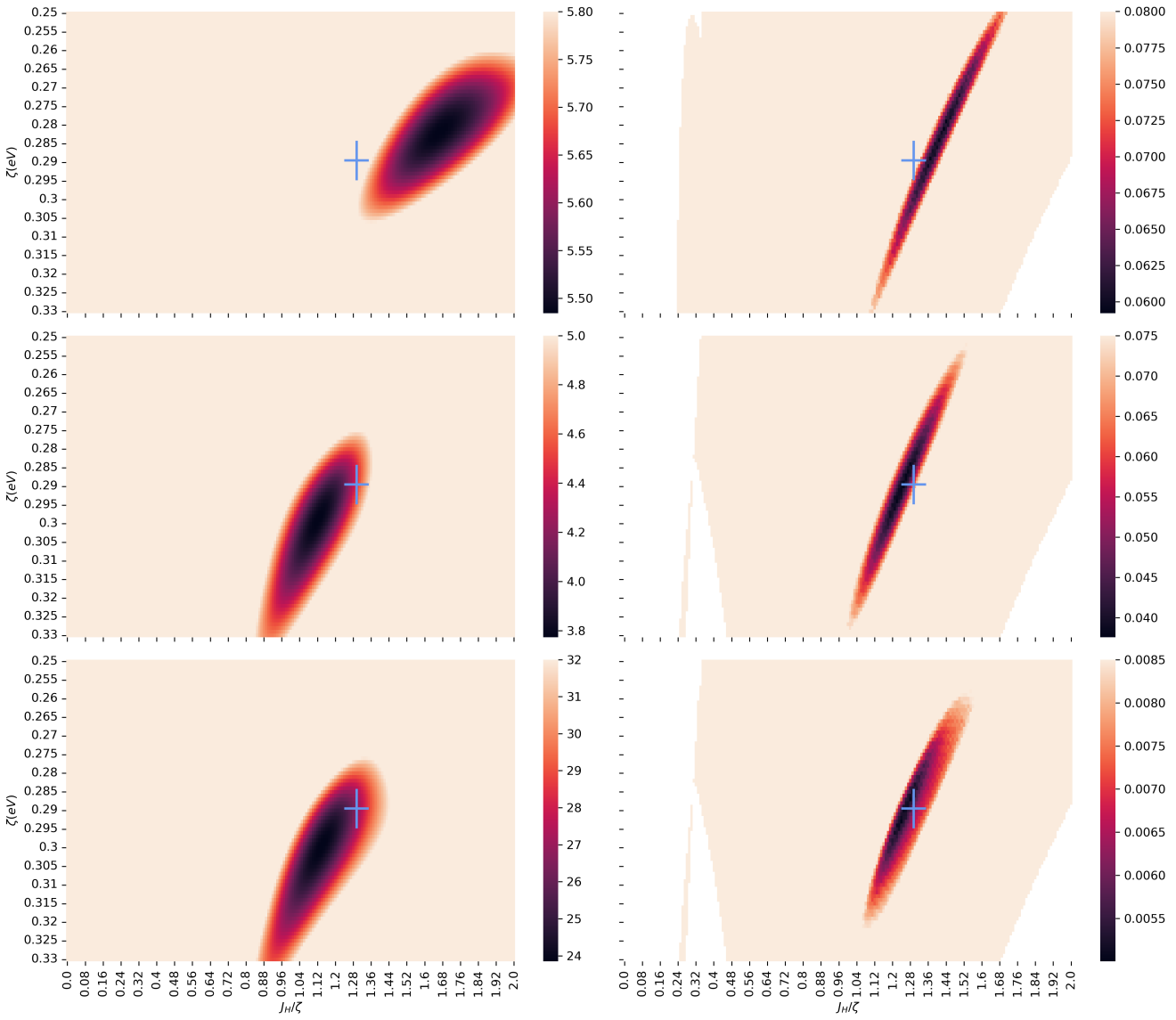

FIG. S7. Heatmaps comparing the calculated and experimental RIXS spectra at resonant E_i for Ba_2YReO_6 within the sampled parameter space of $\zeta \in [0.25, 0.33]$ and $J_H/\zeta \in [0, 2]$. Two metrics are plotted. Left column: the sum of the squared differences between the calculated and experimental spectra intensities. Right column: the sum of the squared differences between the calculated and experimental peak positions in energy transfer. The three rows correspond to the Re L_2 edge (top), the Re L_3 edge (middle), and the Re L_2 edge value times the Re L_3 edge value (bottom). When calculated RIXS spectra do not have the same number of peaks as the experimental data, these are removed from the plot (white regions in the right heatmaps). The blue cross marker denotes the selected optimal values for ζ and J_H/ζ with error bars.

ACKNOWLEDGMENTS

Work at the University of Toronto was supported by the Natural Sciences and Engineering Research Council (NSERC) of Canada through the Discovery Grant No. RGPIN-2019-06449, Canada Foundation for Innovation, and Ontario Research Fund. Work performed at Brookhaven National Laboratory was supported by the U.S. Department of Energy (DOE), Division of Materials Science, under Contract No. DE-SC0012704. This research used resources of the Advanced Photon Source, a U.S. Department of Energy (DOE) Office of Science user facility operated for the DOE Office of Science by Argonne National Laboratory under Contract No. DE-AC02-06CH11357 We acknowledge support from the US National Science Foundation (NSF) Grant Number 2201516 under the Accelnet program of

Office of International Science and Engineering (OISE).

[S1] Y. Wang, G. Fabbris, M. Dean, and G. Kotliar, Edrixs: An open source toolkit for simulating spectra of resonant inelastic x-ray scattering, Computer Physics Communications **243**, 151 (2019).

[S2] R. D. Cowan, *The Theory of Atomic Structure and Spectra*, Los Alamos Series in Basic and Applied Sciences, Vol. 3 (University of California Press, 1981).

[S3] E. König, The nephelauxetic effect calculation and accuracy of the interelectronic repulsion parameters I. Cubic high-spin d2, d3, d7, and d8 systems, in *Structutal and Bonding* (Springer, Berlin, Heidelberg, 1971) pp. 175–212.

[S4] B. Yuan, J. P. Clancy, A. M. Cook, C. M. Thompson, J. Greedan, G. Cao, B. C. Jeon, T. W. Noh, M. H. Upton, D. Casa, T. Gog, A. Paramekanti, and Y.-J. Kim, Determination of hund's coupling in $5d$ oxides using resonant inelastic x-ray scattering, Phys. Rev. B **95**, 235114 (2017).